TU Delft

Delft University of Technology

Document Version
Final published version

Licence
Dutch Copyright Act (Article 25fa)

Citation (APA)
Kariminejad, M. M., Sharifi, M. A., Amiri-Simkooei, A., & Mostafavi, M. A. (2025). Impact of Model Uncertainty and Sensor Deployment Geometry on the Precision of BLE RSSI-Based Indoor Positioning. *IEEE Sensors Journal*, *26*(2), 2181-2193. https://doi.org/10.1109/JSEN.2025.3637898

Important note
To cite this publication, please use the final published version (if applicable).
Please check the document version above.

Copyright
In case the licence states “Dutch Copyright Act (Article 25fa)”, this publication was made available Green Open Access via the TU Delft Institutional Repository pursuant to Dutch Copyright Act (Article 25fa, the Taverne amendment). This provision does not affect copyright ownership.
Unless copyright is transferred by contract or statute, it remains with the copyright holder.

Sharing and reuse
Other than for strictly personal use, it is not permitted to download, forward or distribute the text or part of it, without the consent of the author(s) and/or copyright holder(s), unless the work is under an open content license such as Creative Commons.

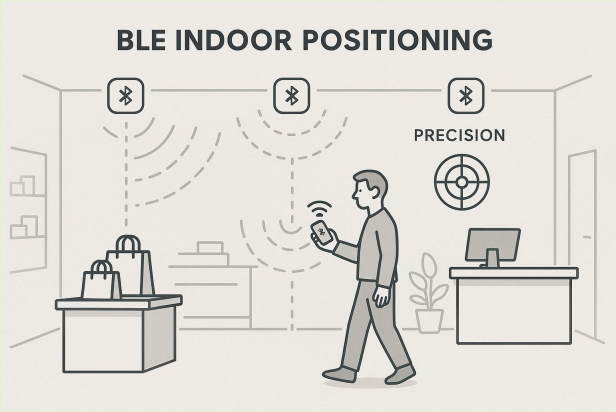
Takedown policy
Please contact us and provide details if you believe this document breaches copyrights.
We will remove access to the work immediately and investigate your claim.

This work is downloaded from Delft University of Technology.

Impact of Model Uncertainty and Sensor Deployment Geometry on the Precision of BLE RSSI-Based Indoor Positioning

Mohammad Mahdi Kariminejad, *Member, IEEE*, Mohammad Ali Sharifi, *Member, IEEE*, Alireza Amiri-Simkooei, *Member, IEEE*, and Mir Abolfazl Mostafavi, *Member, IEEE*

***Abstract*—Indoor positioning systems based on Bluetooth technology have gained significant attention with the widespread adoption of Bluetooth Low Energy (BLE). The rapid growth of BLE-enabled devices—now exceeding eight billion worldwide—has enabled the development of cost-effective, location-aware applications. The precision of BLE indoor positioning systems depends on several factors, among which the quality of received signal strength indicator (RSSI) measurements and the spatial deployment of sensors are most critical. Existing research has largely focused on improving RSSI accuracy through techniques such as multichannel measurements, outlier detection, Kalman filtering, and regression modeling. In this work, we examine two primary components that govern positioning precision: 1) the uncertainty in the RSSI-distance model parameters, including the path-loss exponent, reference power, and raw RSSI values; and 2) the geometry of sensor deployment, which directly affects estimation precision through the geometric dilution of precision (GDoP). We demonstrate that optimizing sensor placement using centroidal Voronoi tessellation (CVT) reduces GDoP and substantially improves positioning precision. Comparative experiments across two deployment scenarios, one based on CVT, confirm that CVT-based sensor configurations yield significantly higher precision in BLE RSSI-based indoor positioning.**



***Index Terms*— Bluetooth Low Energy (BLE), centroidal Voronoi tessellation (CVT), geometric dilution of precision (GDoP), indoor positioning, mathematical model, precision, sensor deployment, uncertainty.**

I. Introduction

RADIO frequency-based indoor positioning systems encompass a wide range of technologies that use radio waves to track or estimate the location of an object. These technologies include Bluetooth Low Energy (BLE) [1], [2], Wireless Fidelity (Wi-Fi) [3], [4], radio frequency identification (RFID) [5], [6], and ultrawideband (UWB) [7], [8]. Each of these has distinct advantages, disadvantages, priorities, limitations, and applications [9]. BLE is favored for low-power and cost-effective applications, particularly in indoor environments where battery life is a critical factor. BLE is typically used in proximity-based systems but may offer lower accuracy compared to other technologies [10]. Wi-Fi is widely available in many environments, making it a convenient option for indoor positioning. However, it is susceptible to multipath effects, where signals bounce off surfaces and cause inaccuracies in distance estimation [11]. RFID is primarily used for asset tracking, offering a simple and effective method for locating tagged objects within a specified area. RFID systems can be passive or active, with passive tags being cheaper and more widely deployed but offering a limited range [12], [13]. UWB provides high accuracy in distance measurement, making it suitable for applications requiring precise localization, such as industrial tracking or indoor navigation [14]. UWB systems are capable of mitigating multipath interference and offering centimeter-level accuracy, though they are more complex and costly to implement [15]. Each of these indoor

Received 2 November 2025; accepted 20 November 2025. Date of publication 8 December 2025; date of current version 14 January 2026. This work was supported by Canada Research Chair in Senseable Cities for Empowered Mobilities through the Natural Sciences and Engineering Research Council of Canada (NSERC). The associate editor coordinating the review of this article and approving it for publication was Prof. Chen Yang. *(Corresponding author: Mohammad Mahdi Kariminejad.)*

Mohammad Mahdi Kariminejad and Mohammad Ali Sharifi are with the School of Surveying and Geospatial Engineering, College of Engineering, University of Tehran, Tehran 1439955961, Iran (e-mail: m.kariminejad@ut.ac.ir; sharifi@ut.ac.ir).

Alireza Amiri-Simkooei is with the Department of Control and Operations, Faculty of Aerospace Engineering, Delft University of Technology (TU Delft), Delft, 2629 HS South Holland, The Netherlands (e-mail: a.amirisimkooei@tudelft.nl).

Mir Abolfazl Mostafavi is with the Department of Geomatic Sciences, Faculty of Forestry, Geography, and Geomatics, Université Laval, Québec City, QC G1V 0A6, Canada (e-mail: mir-abolfazl.mostafavi@scg.ulaval.ca).

Digital Object Identifier 10.1109/JSEN.2025.3637898

1558-1748 © 2025 IEEE. All rights reserved, including rights for text and data mining, and training of artificial intelligence and similar technologies. Personal use is permitted, but republication/redistribution requires IEEE permission.
See https://www.ieee.org/publications/rights/index.html for more information.
Authorized licensed use limited to: TU Delft Library. Downloaded on January 29,2026 at 11:10:50 UTC from IEEE Xplore. Restrictions apply.

positioning technologies has its strengths and weaknesses, and the selection of an appropriate system depends on the specific requirements of the application, including factors such as accuracy, environmental conditions, energy consumption, and cost.

Among the various indoor positioning technologies, BLE has gained significant attention in recent years, largely due to its distinctive advantages, which include low cost, minimal energy consumption, and widespread availability. These characteristics make BLE an increasingly attractive option for a wide range of applications, particularly in environments where energy efficiency and affordability are paramount. BLE's ability to deliver reliable performance with relatively simple hardware and infrastructure requirements further enhances its appeal, especially for indoor positioning systems. BLE relies on received signal strength indicator (RSSI) measurement to estimate the position of devices within an indoor environment [16]. RSSI, which measures the power level of a received radio signal, serves as a fundamental metric for estimating distances between transmitters and receivers. By analyzing the strength of the signal at various locations, BLE systems can infer the relative position of devices or users within a given area. BLE uses RSSI as a core measurement for indoor positioning applications [17]. Furthermore, BLE offers a more energy-efficient alternative, especially suited for applications where battery life is critical, such as in mobile devices, wearable technology, and asset tracking systems. The integration of BLE into many consumer devices, such as smartphones, tablets, and smart home devices, further enhances its utility and adoption for indoor positioning applications.

One of the primary challenges associated with BLE RSSI-based indoor positioning is the precision of the final estimated position. Due to some limitations in RSSI measurement received by low-cost devices similar to smartphones, achieving highly accurate and precise indoor positioning outputs is usually not possible [18]. In this case, the appropriate mathematical model is crucial for improving the final outputs. Uncertainty in mathematical model parameters can directly impact the final precision. On the other hand, BLE beacons transmit signals that attenuate rapidly because of their low-energy intrinsic structure. This challenge causes the limitation in coverage of the BLE signals, and subsequently, the geometry of sensor deployment considering appropriate coverage is so important.

Recent research, regarding improving the accuracy and precision of the final estimated position, focuses on smoothing the raw RSSI measurement, removing the outliers, and using appropriate mathematical models to enhance the quality of final outputs. Among these researches, using multichannel measurement [19], smoothing filter (e.g., Kalman filter) [20], particle swarm optimization [21], Monte Carlo simulation [22], wavelet denoising [23], machine learning (ML) methods [24], [25], and also integration of BLE measurement with other radio or inertial sensors are commonly adopted [26], [27].

The primary research objective of this study is to investigate the crucial components that impact the precision of the final positioning parameters in BLE RSSI-based indoor positioning systems. These critical components are related to the mathematical model and its parameters (as a sensing model part), and also the configuration of BLE sensors (or beacons) deployments (as a coverage model part). By examining these critical elements, the study aims to uncover strategies that can optimize the performance of BLE-based systems, particularly in terms of their precision in real-world indoor positioning applications.

In this research, we proposed two primary components that significantly affect the precision of indoor positioning parameters, namely, the uncertainty of mathematical model parameters and the geometry of sensor configuration indexing by geometric dilution of precision (GDoP) in navigation literature. These components are interdependent and crucial for ensuring accurate and precise results. Mathematical modeling is a key element in interpreting and processing the RSSI measurement from beacons [28]. This aspect of the process involves several essential components, including outlier detection and mitigation, the smoothing of data, and the estimation of parameters within the RSSI-distance model. The model relates the received signal strength to the distance between the transmitter (beacon) and receiver, taking into account environmental factors such as obstacles, signal attenuation, and interference. The process involves using well-known techniques, such as the least-squares method, to estimate critical model parameters, including environmental factor and maximum transmission power. Moreover, the final precision of positioning parameters is significantly influenced by each variance component of the estimated parameters. This research, specifically, aims to provide the analytical form of distance precision obtained from RSSI measurement and then positioning precision using least-squares estimation. Also, in the configuration component, a class of Voronoi diagram method has been adopted to tessellate the area of interest called centroidal Voronoi tessellation (CVT) that maximizes the area between sensors and receivers. This matter causes the geometry dilution of precision minimization.

In summary, the precision of indoor positioning parameters is influenced by a combination of sensing model and coverage model parameters, including mathematical modeling alongside the geometry of sensor deployment strategies. The mathematical model's ability to interpret data accurately, while accounting for factors such as outliers, data smoothing, and environmental variables, is vital for ensuring precise positioning estimates. Additionally, the management of noise and the propagation of errors through the system are crucial factors that should be carefully considered to optimize the overall performance of indoor positioning systems. Furthermore, the GDoP is an important criterion for the positioning output precision investigation.

The remainder of this article is organized as follows. Section II provides a review of relevant literature addressing various elements associated with BLE RSSI-based indoor positioning precision. In Section III, i.e., methodology, we introduce the mathematical relations of two mentioned components that influence the final precision of BLE-based indoor positioning systems. Field experiments, along with their results, are detailed in Section IV. Finally, Section V

Authorized licensed use limited to: TU Delft Library. Downloaded on January 29,2026 at 11:10:50 UTC from IEEE Xplore. Restrictions apply.

concludes this article and outlines directions for future research.

II. Literature Review

The precision of indoor positioning systems using low-cost radio sensors, such as BLE, is an important topic that many researchers in academia and industry are investigating due to the efficiency and widespread use of wireless communication. The literature on high-precision indoor positioning systems presents a wide array of technological innovations and methodologies designed to enhance accuracy and reliability in various indoor environments. UWB technology is frequently highlighted, with several studies, including those by Ling et al. [29], Mazhar et al. [14], and Guo et al. [30], emphasizing its effectiveness in providing centimeter-level precision, particularly in complex indoor settings. UWB's potential is further enhanced by advanced algorithms, such as particle filtering [31], which optimizes the handling of both line-of-sight (LoS) and non-LoSt (NLoS) conditions, and filtering techniques like Kalman and median filters [15], which stabilize range measurement and reduce noise. Additionally, the application of UWB technology in multiuser scenarios is explored by Yin et al. [32], who propose waveform division multiple access to enhance positioning accuracy in crowded environments.

Complementing UWB systems, IMU-based techniques, like the one proposed by Bai et al. [33], offer precise pedestrian positioning by incorporating motion speed-based adaptive error compensation and step detection, thus improving accuracy without the need for additional sensors. Vision-based approaches are also prominent, with Yang et al. [34] introducing a pixel threshold-based eight-point method and De-La-Llana-Calvo et al. [35] assessing AoA-based positioning using lighting infrastructure and position-sensitive detectors. These techniques contribute to the growing body of research focused on enhancing positioning accuracy with visual and optical methods. In a similar vein, systems that leverage visible light communication (VLC), such as the one proposed by Cai et al. [36] using particle swarm optimization, show promise for achieving high-precision 3-D positioning. Pseudolite-based systems are another significant area of focus, with Gan et al. [37] introducing array pseudolite technology for improved precision and Zhao et al. [38] addressing the challenge of eliminating the need for known point initialization in pseudolite-based positioning systems.

Moreover, Grasso et al. [39] examine the performance, precision, and failure rates of UWB-based 2-D positioning systems, using time-difference-of-arrival (TDoA) signals and multilateration techniques, while Seong et al. [40] propose a robust RTT-based indoor positioning system that incorporates RTT compensation and a region proposal network (RPN). Meanwhile, emerging technologies such as 5G are also gaining attention; Gao et al. [41] demonstrate how 5G's multilevel feature synthesis method can be utilized to achieve high-precision positioning in both indoor and urban environments. Furthermore, comprehensive reviews by Qiao et al. [42], Elsanhoury et al. [43], and Barnes et al. [44] provide valuable insights into the evolution and future potential of UWB, Wi-Fi, and pseudolite technologies in indoor positioning, especially in the context of IoT and urban applications. Collectively, these studies illustrate the growing trend toward hybrid positioning systems that integrate multiple technologies—such as UWB, vision, VLC, pseudolites, and 5G—to overcome the inherent challenges of indoor localization, offering more accurate, reliable, and versatile solutions for a variety of applications.

For BLE indoor positioning accuracy and precision improvement much literature focuses on enhancing the RSSI measurement by employing multichannel signals or using mathematical techniques such as outlier detection and mitigation, Kalman filter smoothing, and identifying appropriate regression models for improving them [23], [28], [45].

One of the most important topics in the precision of positioning systems is the dilution of precision, which is related to the geometry of sensor deployment. DoP, first introduced by Langley et al. [46], is a critical concept in positioning systems, reflecting how receiver–transmitter geometry influences the precision of location estimates. Langley defined several variations of DoP, including geometric DoP (GDoP), position DoP (PDoP), horizontal DoP (HDoP), vertical DoP (VDoP), and time DoP (TDoP), apply to different aspects of positioning and timing. Recent studies have extended this concept across various positioning technologies. For instance, Dwi Ramadhani et al. [47] proposed a weighted GDoP (WGDOP) method for improved localization in systems like UWB, while Wang et al. [48] focused on DoP in indoor positioning using the TDoA technique. Sharp et al. [49] and Küçük [50] further investigated DoP in indoor systems, examining the influence of multipath and NLoS conditions on positioning accuracy. Additionally, Albaidhani and Alsudani [51] proposed selecting anchor nodes based on GDoP to optimize UWB positioning, while Khalife and Kassas [52] introduced an optimization algorithm to minimize DoP for sensor deployment. Studies like Guo et al. [53] combined DoP with Kalman filters for enhanced UWB positioning, and Wang et al. [54] and Zhang and Lu [55] analyzed the impact of DoP in 3-D AoA systems, highlighting its importance in improving positioning precision in wireless sensor networks and indoor environments. Collectively, this body of work emphasizes the critical role of DoP in optimizing the accuracy of modern positioning systems through improved sensor deployment, advanced filtering, and geometrical considerations.

Also, the Voronoi diagram is a widely used method for spatial tessellation in various applications, particularly in indoor positioning and navigation systems. It has been applied to improve the accuracy and efficiency of localization algorithms in wireless sensor networks. For instance, Hao et al. [56] developed an algorithm based on the Voronoi diagram and support vector machines to enhance the localization of wireless nodes for disaster monitoring and management. Hobby and Dashti [57] applied the Voronoi diagram to indoor location tracking systems using Wi-Fi measurement, while Yong et al. [58] introduced a novel fingerprint interpolation technique for radio map construction, utilizing Voronoi diagrams and reference point (RP) clustering to generate virtual fingerprints, thereby improving the accuracy of

Authorized licensed use limited to: TU Delft Library. Downloaded on January 29,2026 at 11:10:50 UTC from IEEE Xplore. Restrictions apply.

indoor positioning by overcoming site survey challenges. Yang et al. [59] proposed a 3-D Voronoi-based sequence localization correction algorithm (SLC3V), which optimizes location estimates in 3-D spaces using RSSI values from beacon nodes. Similarly, Afghantoloee and Mostafavi [60] proposed a local optimization algorithm based on a 3-D Voronoi diagram to define sensor proximity relationships in 3-D indoor environments. Freidman et al. [61] introduced Voronoi random fields (VRFs) as a technique for mapping the topological structure of indoor spaces, capturing both spatial layout and connectivity. Furthermore, Onishi [62] used Voronoi tessellation (VT) for BLE indoor positioning, demonstrating its utility in enhancing BLE-based localization systems. Collectively, these studies highlight the versatility of Voronoi diagrams in improving the performance and accuracy of indoor positioning systems across various technologies and approaches.

Among them, the centroidal Voronoi diagram has been widely applied in various fields, including indoor positioning, thanks to its ability to optimize spatial distributions. Du et al. [63] first introduced CVT, which has since been applied to problems in image compression, quadrature, and resource distribution. Their subsequent work, such as [64], demonstrated the use of CVT in grid generation for finite element approximations of partial differential equations. Ju et al. [65] further advanced CVT by presenting probabilistic methods for their determination and parallel implementations, offering more accurate and efficient approximations without explicitly constructing Voronoi diagrams. Du and Wang [66] explored the asymptotic structures of optimal CVT, contributing to the theoretical understanding of their behavior, while they provided a precise definition of constrained CVT (CCVT) and algorithms for their construction [67]. They also analyzed the convergence of the popular Lloyd algorithm for CVT computation, which, despite its widespread use, was found to have incomplete theoretical analysis [68]. Later, Liu et al. [69] proposed more efficient CVT computation methods with faster convergence, particularly for convex domains with smooth density. Additionally, Lévy and Liu [70] examined CVT in the L_p norm using quasi-Newton optimization, demonstrating their application in simulation problems. These advancements have significantly improved the efficiency and application of CVT in various fields, including indoor positioning, where their optimal spatial distribution properties can enhance localization precision.

In this study, we aim to address two distinguish components that directly impact the precision of BLE RSSI-based indoor positioning systems. The first one is the uncertainty of mathematical model parameters, which propagates into the distance uncertainty and then positioning components using a nonlinear error propagation law. The error propagation method has been widely employed in the scientific literature for analyzing the propagation of uncertainties [71]. This challenge shows itself in defining the RSSI-distance model parameters more accurately. The second is to design a specific sensor deployment that minimizes the GDoP to improve output precision. For this purpose, we propose a class of Voronoi diagram tessellations, specifically CVT, and implement them using Lloyd's algorithm optimization for a distinct sensor deployment scenario. Additionally, we compare its efficiency against an arbitrary sensor deployment for performance evaluation.

III. Methodology

In this section, we explicitly introduced the components that impact the precision of indoor positioning parameters. These include the uncertainty of mathematical model parameters and the geometry of sensor deployment.

A. Uncertainty of Mathematical Model Parameters

1) Distance Precision Calculated From RSSI Measurement:

In this context, the mathematical model is defined based on the combination of functional model and stochastic model of RSSI measurement. The functional model is introduced based on the signal propagation of BLE beacons throughout an environment. This obeys a logarithm model as follows [72]:

$$\mathrm{RSSI} = -10\,n\,\log_{10}\left(\frac{d}{d_0}\right) + P_0 + X_\sigma \tag{1}$$

where d denotes the distance between the transmitter and the receiver and n represents the path-loss exponent, which depends on the characteristics of the wireless transmission environment. A greater number of obstacles typically results in a higher value of n. The term P_0 corresponds to the RSSI at a reference distance d_0 from the transmitter. X_σ is a random variable following a Gaussian distribution with a mean of zero and a variance of σ^2. For computational convenience, the reference distance d_0 is typically set to 1 m. Given that X_σ has a mean of zero, the distance-dependent path-loss model can be rewritten as follows:

$$\rho = -10\,\nu\,\log_{10}(d) - \mu \tag{2}$$

where ρ represents the received signal strength values received by the antenna, d denotes the distance between the transmitters (beacons) and the receiver, ν is the environmental factor that characterizes the path-loss exponent, and μ denotes the maximum transmission power of a beacon measured at a reference distance of 1 m. The above formulation can be transformed as follows:

$$d = 10^{\frac{\rho+\mu}{-10\nu}}. \tag{3}$$

The covariance matrix of the distance can be derived from the covariance matrix of the $y = [\rho, \mu, \nu]^T$ using the law of error propagation as follows:

$$\mathbf{Q}_d = \mathbf{J}\,\mathbf{Q}_y\,\mathbf{J}^T \tag{4}$$

where

$$\mathbf{Q}_y = \begin{pmatrix} \sigma_\rho^2 & \sigma_{\rho\mu} & \sigma_{\rho\nu} \\ \sigma_{\mu\rho} & \sigma_\mu^2 & \sigma_{\mu\nu} \\ \sigma_{\nu\rho} & \sigma_{\nu\mu} & \sigma_\nu^2 \end{pmatrix} \tag{5}$$

Authorized licensed use limited to: TU Delft Library. Downloaded on January 29,2026 at 11:10:50 UTC from IEEE Xplore. Restrictions apply.

denotes the covariance matrix of vector y, $\mathbf{Q}_d = \sigma_d^2$ denotes the variance of the distance, and $\mathbf{J}$ is Jacobian vector defined here as follows:

$$\mathbf{J} = \left(\frac{\partial d}{\partial \rho} \ \frac{\partial d}{\partial \mu} \ \frac{\partial d}{\partial \nu}\right). \tag{6}$$

The above differentiation components are given as follows:

$$\frac{\partial d}{\partial \rho} = -\frac{\ln 10 \ \cdot \ 10^{\frac{\rho+\mu}{-10\nu}-1}}{\nu} \tag{7}$$

$$\frac{\partial d}{\partial \mu} = -\frac{\ln 10 \ \cdot \ 10^{\frac{\rho+\mu}{-10\nu}-1}}{\nu} \tag{8}$$

$$\frac{\partial d}{\partial \nu} = \frac{\ln 10 \ \cdot \ (\rho+\mu) \ \cdot \ 10^{\frac{\rho+\mu}{-10\nu}-1}}{\nu^2} \tag{9}$$

where ∂ represents the partial differentiation operator. After some mathematical simplifications, we have

$$\begin{aligned}\sigma_d^2 = \ & \sigma_\rho^2 \left(\frac{\partial d}{\partial \rho}\right)^2 + \sigma_\mu^2 \left(\frac{\partial d}{\partial \mu}\right)^2 + \sigma_\nu^2 \left(\frac{\partial d}{\partial \nu}\right)^2 \\ & + 2\sigma_{\rho\mu} \left(\frac{\partial d}{\partial \rho}\frac{\partial d}{\partial \mu}\right) + 2\sigma_{\rho\nu} \left(\frac{\partial d}{\partial \rho}\frac{\partial d}{\partial \nu}\right) \\ & + 2\sigma_{\mu\nu} \left(\frac{\partial d}{\partial \mu}\frac{\partial d}{\partial \nu}\right).\end{aligned} \tag{10}$$

Subsequently, after substituting (7)–(9) into (10), the expression for the precision of the distance can be obtained as follows, (11), as shown at the bottom of the next page, or simply

$$\begin{aligned}\sigma_d = \pm\frac{\ln(10)\ d}{10\nu}\Big[\sigma_\rho^2 + \sigma_\mu^2 + \left(10\log_{10}(d)\right)^2\sigma_\nu^2 + 2\sigma_{\rho\mu} \\ +20\log_{10}(d)\ \left(\sigma_{\rho\nu} + \sigma_{\mu\nu}\right)\Big]^{\frac{1}{2}}.\end{aligned} \tag{12}$$

The RSSI noise exhibits temporal correlation, yielding colored noise and subsequently statistically dependent model parameters, which produce a full covariance matrix. In a simplified approach, however, the covariance matrix is assumed to be diagonal and the cross-covariance terms are neglected as follows:

$$\mathbf{Q}_y = \begin{pmatrix}\sigma_\rho^2 & 0 & 0 \\ 0 & \sigma_\mu^2 & 0 \\ 0 & 0 & \sigma_\nu^2\end{pmatrix}. \tag{13}$$

Neglecting the cross-covariance components, (11) gives the distance standard deviation as

$$\sigma_d = \pm\sqrt{\frac{(\ln 10)^2\ 10^{\frac{\rho+\mu}{-5\nu}-2}}{\nu^2}\left[\sigma_\rho^2 + \sigma_\mu^2 + \frac{(\rho+\mu)^2}{\nu^2}\sigma_\nu^2\right]} \tag{14}$$

or

$$\sigma_d = \pm\frac{\ln 10 \cdot d}{10\nu}\left(\sigma_\rho^2 + \sigma_\mu^2 + \left(10 \cdot \log_{10}(d)\right)^2\sigma_\nu^2\right)^{\frac{1}{2}}. \tag{15}$$

2) Positioning Parameters Precision: By considering the 3-D Euclidean distance, (2) can be rewritten in the following form:

$$\rho = -10\ \nu\ \log_{10}\sqrt{(x_b - x_r)^2 + (y_b - y_r)^2 + (z_b - z_r)^2} - \mu \tag{16}$$

where $[x_b, y_b, z_b]^T$ is the position of the beacon and $[x_r, y_r, z_r]^T$ is the receiver position. As a combined nonlinear model, we can reformulate the above equation in the Gauss–Helmert model as follows:

$$\begin{aligned}f(x, y) = & \ 10^{\frac{\rho+\mu}{-10\nu}} \\ & - \sqrt{(x_b - x_r)^2 + (y_b - y_r)^2 + (z_b - z_r)^2} = 0\end{aligned} \tag{17}$$

where y, i.e., $[\rho, \mu, \nu]^T$ can be considered as an observation vector and $x = [x_r, y_r, z_r]^T$ can be considered as the unknown parameters. After the first-order linearization, we have [73]

$$f(x_0, y_0) + \frac{\partial f}{\partial p}|_{x=x_0}(x - x_0) + \frac{\partial f}{\partial q}|_{y=y_0}(y - y_0) = 0 \tag{18}$$

where y_0 and x_0 are the initial values of the observation and unknown parameters vector, respectively. $f(x_0, y_0)$ calls the *misclosure vector* denotes by w, $\partial f/\partial y|_{y=y_0}$ calls the *design matrix of observation* denotes by $\mathbf{B}$, and $\partial f/\partial x|_{x=x_0}$ calls the *design matrix of unknown parameters* denoted by $\mathbf{A}$. We renotation (17) as follows:

$$f(x, y) = \mathbf{A}\delta x + \mathbf{B}\delta y + w = 0 \tag{19}$$

where the ith column of the design matrices of observation and unknown parameters is

$$\mathbf{A}_i = \left(\frac{x_{r_i} - x_b}{d_i} \ \frac{y_{r_i} - y_b}{d_i} \ \frac{z_{r_i} - z_b}{d_i}\right) \tag{20}$$

$$\mathbf{B}_i = \left(-\frac{\ln 10\, d_i}{10\nu} \ -\frac{\ln 10\, d_i}{10\nu} \ -\frac{\ln 10\ (\rho+\mu)\ d_i}{10\nu^2}\right). \tag{21}$$

The weighted least-squares estimation of unknown parameters in the Gauss–Helmert model is as follows [74]:

$$\hat{x} = \left(\mathbf{A}^T\left(\mathbf{B}\ \mathbf{Q}_y\mathbf{B}^T\right)^{-1}\mathbf{A}\right)^{-1}\mathbf{A}^T\left(\mathbf{B}\ \mathbf{Q}_y\mathbf{B}^T\right)^{-1}w. \tag{22}$$

Subsequently, the precision of the positioning parameters can be expressed as follows:

$$\mathbf{Q}_{\hat{x}} = \left(\mathbf{A}^T\left(\mathbf{B}\ \mathbf{Q}_y\mathbf{B}^T\right)^{-1}\mathbf{A}\right)^{-1}. \tag{23}$$

The above formulation offers a linear approximation of the positioning parameter precision. This approximation may be further refined through the inclusion of higher order linearization terms. The methodology for computing parameters and their associated precisions within the Gauss–Helmert model is detailed in [74] and [75].

B. Geometry of Sensor Deployment

1) Geometric Dilution of Precision (GDoP): An essential component influencing the accuracy and precision of positioning parameters is the geometry of sensor deployment within a geospatial system. In the context of radio navigation, this geometric influence is commonly quantified through a measure known as the GDoP. This refers to the level of uncertainty in the determination of a receiver's position, which arises as a function of the relative spatial arrangement of the sensors involved in the measurement process. To illustrate, consider

Authorized licensed use limited to: TU Delft Library. Downloaded on January 29,2026 at 11:10:50 UTC from IEEE Xplore. Restrictions apply.

a radio positioning system in which a receiver is tasked with determining its position by measuring the distances to two terrestrial transmitters, with the objective of computing its horizontal coordinates. In this scenario, the receiver's location is determined by the intersection of two circular lines of position, each centered on one of the transmitters, with the radius of each circle corresponding to the measured range from the receiver to the respective transmitter (as depicted in Fig. 1). However, due to the inherent inaccuracies in the measurement of the ranges, these lines of position will not precisely coincide with the true location of the receiver. As a result, the intersection of the circles will be displaced from the actual receiver location, introducing an error in the computed position. The magnitude of this error is heavily influenced by the geometric configuration of the transmitter–receiver system. Specifically, the relative distances and angles between the receiver and the transmitters play a critical role in determining the degree of positional uncertainty. When the transmitters are positioned in a way that results in a favorable geometry, such as being spread out across a wide area, the uncertainty in the receiver's position will be lower, leading to a more precise estimate. Conversely, when the transmitters are situated in close proximity or along nearly collinear paths, the positioning accuracy will deteriorate, as the intersection of the range circles becomes less distinct, and the error in the position estimate increases. Thus, the geometry of the sensor arrangement is a key factor in determining the overall precision of the radio positioning system. In Fig. 1(a), the sensors are positioned at a relatively large distance from one another, which results in a smaller region within which the receiver's location can be determined with a given level of certainty. The positioning of Sensor 1 is nearly orthogonal to the direction of Sensor 2, leading to a situation where the receiver's X and Y coordinates can be determined with approximately equal precision. This favorable geometric arrangement minimizes the uncertainty in both coordinate directions, and the receiver's position can be estimated with high precision. In contrast, Fig. 1(b) depicts a scenario in which the sensors are positioned much closer together. This closer proximity results in a significantly larger region of uncertainty, within which the receiver's position could lie. In this configuration, the uncertainty in the determination of the Y coordinate is notably larger than that of the X coordinate, meaning that the Y coordinate is less precise than the X coordinate. As a consequence, the overall precision of the position estimate deteriorates when compared to the configuration shown in Fig. 1(a). This difference in precision between the two configurations is indicative of what is referred to as DoP. Specifically, in (b), the precision of the positioning estimate is said to be "diluted" in comparison to (a). This term reflects the increased uncertainty in the position estimate that results from the less favorable geometry of the sensor deployment in Fig. 1(b). The closer proximity of the sensors in this

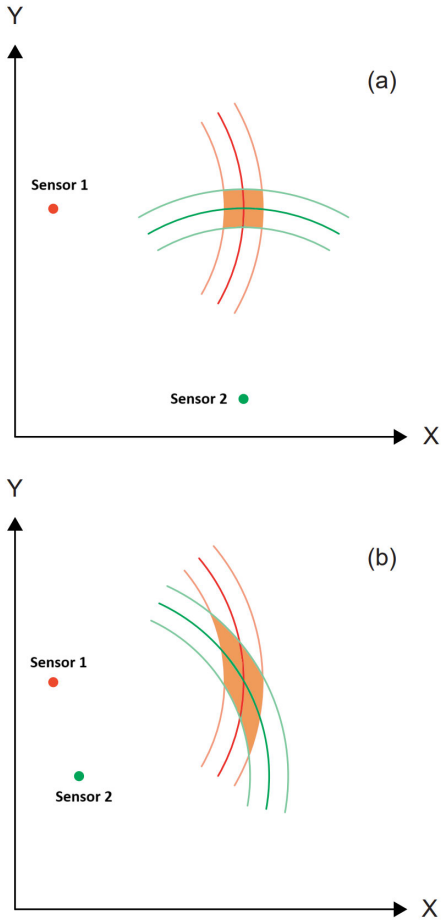


Fig. 1. Two types of sensor deployments and their respective areas of uncertainty.(a) Position uncertainty is small (low dilution of precision). (b) Sensor 2 is moved closer to Sensor 1, and although the measurement uncertainty remains the same, the position uncertainty is considerably larger (high dilution of precision).

case diminishes the ability to precisely determine the receiver's position, particularly along the Y axis, thus leading to a less reliable measurement overall. Consequently, the positioning precision is significantly reduced in configuration (b) relative to configuration (a), highlighting the critical importance of sensor geometry in determining the precision of radio-based positioning systems. Based on the estimated covariance matrix given in (23), we have

$$\mathbf{Q}_{\hat{x}} = \begin{pmatrix} \sigma_{x_r}^2 & \sigma_{x_r y_r} & \sigma_{x_r z_r} \\ \sigma_{y_r x_r} & \sigma_{y_r}^2 & \sigma_{y_r z_r} \\ \sigma_{z_r x_r} & \sigma_{z_r y_r} & \sigma_{z_r}^2 \end{pmatrix} \tag{24}$$

where the diagonal elements (σ^2) represent the estimated variances of the receiver's 3-D positioning parameters, while the off-diagonal elements correspond to the associated covariance components. In this context, larger estimated variances

$$\sigma_d = \pm \sqrt{\frac{(\ln 10)^2 \ 10^{\frac{\rho+\mu}{-5\nu}-2}}{\nu^2} \left[\sigma_\rho^2 + \sigma_\mu^2 + \frac{(\rho+\mu)^2}{\nu^2} \sigma_\nu^2 + 2\sigma_{\rho\mu} - 2\frac{(\rho+\mu)}{\nu} \left(\sigma_{\rho\nu} + \sigma_{\mu\nu} \right) \right]} \tag{11}$$

Authorized licensed use limited to: TU Delft Library. Downloaded on January 29,2026 at 11:10:50 UTC from IEEE Xplore. Restrictions apply.

indicate lower precision in the estimated positions. We can also define the GDoP based on estimated variances as follows:

$$\text{GDoP} = \sqrt{\sigma_{x_r}^2 + \sigma_{y_r}^2 + \sigma_{z_r}^2} \tag{25}$$

where a lower GDoP indicates greater precision in the estimation of the receiver's coordinates. Consequently, we should seek a specific sensor deployment to cause the minimum GDoP. In this article, we have proposed a class of Voronoi diagram to create a homogeneous sensor network that can satisfy the above condition. This sensor deployment is based on CVT, where each sensor is iteratively deployed at the centroid of each polygon. This method is theoretically reviewed in Sections III-B.2. Here, since (22) is influenced by the RSSI noise, the GDoP metric consequently depends on both the geometric configuration and the statistical characteristics of the assumed RSSI noise.

2) Centroidal VT (CVT): First, let us review the definition of CVT in Euclidean space. We start with a specified open bounded domain $\Omega \in \mathbb{R}^k$ and a set of distinct points $\{\xi_i\}_{i=1}^k \subset \Omega$. For each point ξ_i, $i = 1, \ldots, k$ define the corresponding Voronoi region V_i, $i = 1, \ldots, k$, by

$$V_i = \left\{\xi \in \Omega \mid \|\xi - \xi_i\| < \|\xi - \xi_j\| \text{ for } j = 1, \ldots, k \text{ and } j \neq i\right\} \tag{26}$$

where $\|.\|$ denotes the Euclidean distance (the L^2 metric) in $\mathbb{R}^k$. Clearly $V_i \cap V_j = \emptyset$ for $i \neq j$, and $\cup_{i=1}^k \overline{V}_i = \overline{\Omega}$ so that $\{V_i\}_{i=1}^k$ is a *tessellation* of Ω. The $\{V_i\}_{i=1}^k$ usually refer as the VT of Ω associated with the point set $\{\xi_i\}_{i=1}^k$. A point ξ_i is called a *generator*; a subdomain $V_i \subset \Omega$ is referred to as the *Voronoi region* (or *Voronoi diagram*) corresponding to the generator ξ_i. Consider a density function $\varrho(x) \geq 0$ defined on Ω; for any region $V \subset \Omega$, the standard mass center (or centroid) ξ^* of V is defined as follows [76]:

$$\xi^* = \frac{\int_V \xi\, \varrho\,(\xi)\, d\xi}{\int_V \varrho\,(\xi)\, d\xi}. \tag{27}$$

Then, a special family of VTs, namely centroidal, is defined. A VT $\{\xi_i, V_i\}_{i=1}^k$ of Ω is a CVT if and only if the generator points associated with Voronoi regions are also the centroids of those regions. This means $\xi_i = \xi_i^*$ for $i = 1, \ldots, k$. Fig. 2 shows two different tessellations for ten normally distributed points within a unit square: the one on the left is based on the classical VT, while the one on the right is based on CVT. As clearly shown in the figure, the points in the right tessellation are homogeneously scattered. If we designate one of these points as a receiver and the others as transmitters, the lower GDoP can be understood. Several computational algorithms are available for the generation of CVTs. Among these, Lloyd's algorithm—commonly employed in the context of K-means clustering—represents a widely used iterative approach for achieving CVT configurations. Alternatively, more advanced optimization techniques, such as quasi-Newton methods (e.g., the Broyden–Fletcher–Goldfarb–Shanno (BFGS) algorithm), may also be applied to efficiently compute optimal centroidal tessellations by leveraging gradient-based optimization principles.

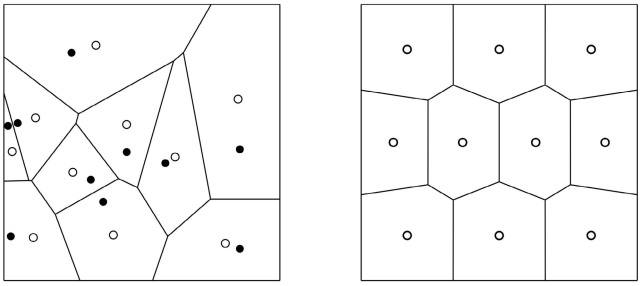


Fig. 2. (Left) VT of the unit square is shown with ten randomly selected generators (represented by the black dots). The white circles indicate the centroids, which do not coincide with the generators. (Right Figure) Additionally, a ten-point CVT of the square, based on a uniform density, is presented [63], [64].

IV. Field Experiments

A. Experimental Setup and GDoP Evaluation

To assess the impact of two primary components on the precision of indoor positioning systems, we employed the Screw-on Bluetooth[1] IT002 beacons—the latest generation of Bluetooth beacons developed by Tatwah. These beacons are fully compliant with the Bluetooth 5.0 standard and are meticulously engineered to accommodate a wide range of applications, including asset tracking, logistics, inventory management, and predictive maintenance, as illustrated in Fig. 3. Subsequently, we conducted a series of controlled experiments within the metrology laboratory at Laval University, located in Québec City, Canada. This setting provided an optimal environment for the precise deployment of sensors on a gridded wall, allowing for a high degree of accuracy in our measurement. The wall is flat, measuring 4×4 m, and is marked with a designated tag for sensor deployment and camera calibration, enabling the precise determination of coordinates, distances, and measurements simultaneously. The experiments were conducted under two distinct sensor deployment scenarios, as depicted in Fig. 4. The first scenario employed the traditional Voronoi diagram approach, while the second utilized CVT. To determine the positions of the sensors in each scenario, a unit square with a side length of 4 m was considered. In Scenario 1, the sensors were placed arbitrarily, and the wall was subsequently tessellated based on the Voronoi diagram. In Scenario 2, following the initial placement of the sensors, the iterative Lloyd's algorithm was applied to obtain the final sensor positions according to the CVT. In both scenarios, the receiver was positioned at the center of the wall. To ensure the accuracy of beacon placement, the locations of the BLE beacons were meticulously fixed along the wall using surveying equipment. We then carefully measured and documented the exact positions of both the BLE beacons and the receiver along the wall, as detailed in Tables I and II.

In order to perform a comprehensive and detailed assessment of position precision, it is essential to calculate the GDoP for each sensor deployment. This calculation allows for an in-depth understanding of the spatial configuration of the sensors, providing valuable insight into the quality of the

[1] Registered trademark.

Authorized licensed use limited to: TU Delft Library. Downloaded on January 29,2026 at 11:10:50 UTC from IEEE Xplore. Restrictions apply.



Fig. 3. Sample of IT002 BLE beacon.

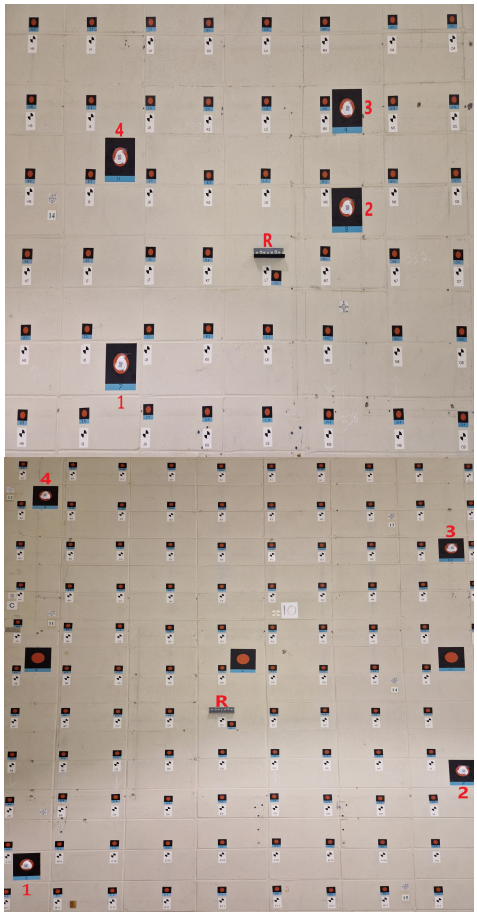


Fig. 4. Scenario 1 sensor deployment (on the top) and Scenario 2 sensor deployment (on the bottom), where the red numbers represent the beacon numbers and "R" denotes the receiver.

TABLE I
COORDINATES OF BLE BEACONS AND RECEIVER IN SCENARIO 1

Device	X (m)	Y (m)
Beacon 1	0	0
Beacon 2	1.14	0.62
Beacon 3	1.14	1.01
Beacon 4	0	0.82
Receiver	0.72	0.41

position estimates. By evaluating the GDoP, we can assess the impact of sensor placement on the overall precision, thereby enabling a more informed analysis of the effectiveness and reliability of each sensor deployment. In our experiment, we know the precise distances between each beacon and receiver, and then we can extract the GDoP for each scenario separately. GDoP is less in the CVT scenario as we expect and mentioned previously. This assessment was provided in Table III. Furthermore, the RSSI values between each beacon and receiver were measured over a 1-min interval at a rate of 0.5 Hz for both scenarios. This duration ensures sufficient data collection to improve the accuracy of distance estimation between each beacon and receiver.

TABLE II
COORDINATES OF BLE BEACONS AND RECEIVER IN SCENARIO 2

Device	X (m)	Y (m)
Beacon 1	0	0
Beacon 2	2.43	0.62
Beacon 3	2.43	2.14
Beacon 4	0	2.60
Receiver	1.10	1.02

TABLE III
GDOP BASED ON THE FIXED COORDINATE FRAME

Scenario	GDoP Value
Scenario 1	1.1878
Scenario 2	1.0252

B. Results and Discussion

1) Distance Precision Calculation: The distance precision for both scenarios was calculated using the error propagation law. Based on the preliminary analysis, we assume the same variances for ρ and μ ($\sigma_\rho = \sigma_\mu = 0.1565$), and also for ν, we assume $\sigma_\nu = 0.03$. In this case, the covariance matrix is assumed to be a diagonal matrix, where the covariance between parameters is absent. The noise is assumed to be Gaussian and independent (white noise), and the measurements are considered free of blunders or outliers, i.e., they are unbiased. In real cases, the indoor positioning problem usually encounters multipath effects due to complex structures; consequently, the noise exhibits temporal correlation (colored noise), and the covariance matrix should be considered nondiagonal (full), where the parameters of the functional model display stochastic dependence. These parameters must be reidentified for each site individually. The covariance matrix of functional model parameters is as follows:

$$\mathbf{Q}_y = \begin{pmatrix} 0.0245 & 0 & 0 \\ 0 & 0.0245 & 0 \\ 0 & 0 & 0.0009 \end{pmatrix}. \tag{28}$$

After applying the error propagation law, the standard deviations for each distance in both scenarios are presented in Tables IV and V, where distance i in the tables denotes the distance between the receiver and the ith beacon. The results indicate that, in Scenario 1 (classical Voronoi diagram), the precision of the distances is higher due to the closer spacing between the beacons and the receiver.

A simulation was conducted to evaluate the precision of distance calculation for various RSSI values, with the mathematical parameters set as $\mu = 65$ and $\nu = 2$. The variances of

Authorized licensed use limited to: TU Delft Library. Downloaded on January 29,2026 at 11:10:50 UTC from IEEE Xplore. Restrictions apply.

TABLE IV
STANDARD DEVIATION OF THE DISTANCES BETWEEN EACH BEACON AND THE RECEIVER IN SCENARIO 1

Distance	Standard Deviation (m)
Distance 1	0.0625
Distance 2	0.0073
Distance 3	0.0250
Distance 4	0.0499

TABLE V
STANDARD DEVIATION OF THE DISTANCES BETWEEN EACH BEACON AND THE RECEIVER IN SCENARIO 2

Distance	Standard Deviation (m)
Distance 1	0.4575
Distance 2	0.3176
Distance 3	0.7357
Distance 4	0.9256

these parameters were assumed to be similar to that of $\mathbf{Q}_y$. The analytical expression for the distance standard deviation, i.e., (14), has been reformulated into two principal components: the linear and nonlinear terms, as detailed in the following:

$$\sigma_d = \pm\sqrt{a_1 a_2}. \tag{29}$$

The linear term (a_1) is expressed as follows:

$$a_1 = \sigma_\rho^2 + \sigma_\mu^2 + \frac{(\rho+\mu)^2}{\nu^2}\sigma_\nu^2. \tag{30}$$

Also, the nonlinear term (a_2) is expressed as follows:

$$a_2 = \frac{(\ln 10)^2\ 10^{\frac{\rho+\mu}{-5\nu}-2}}{\nu^2}. \tag{31}$$

To facilitate a clearer understanding of the linear and nonlinear components, as well as the overall behavior of the distance standard deviation, the variations of these terms over the range of RSSI values from -100 to $+100$ dbm are illustrated in Figs. 5–7. The y-axes in these figures were plotted on a logarithmic scale to enhance clarity and better illustrate variations across a wide range of values, while the x-axes were plotted on a linear scale.

It is logically expected that, within the linear component, the absolute minimum value occurs when RSSI $= \mu$. On the other hand, due to the inherent nature of the exponential function in the nonlinear component, its value decreases smoothly over the considered range. By combining these two components, the resulting standard deviation plot demonstrates that as the distance between the beacon and the receiver decreases, the precision of the distance estimation improves. Consequently, we aim to demonstrate an important finding: even with poor geometric configurations, the distance precision can remain high. This outcome is primarily attributed to shorter intersensor distances. Nevertheless, alongside the precision derived from the model uncertainty, the geometric arrangement of the sensor deployment plays a crucial role in the final estimated precision. This simulation is consistent with the results calculated for our case study, as presented in Tables IV and V.

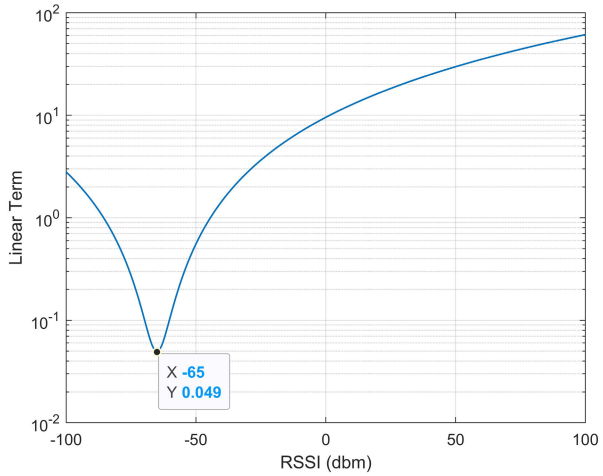


Fig. 5. Linear term of the distance standard deviation formula.

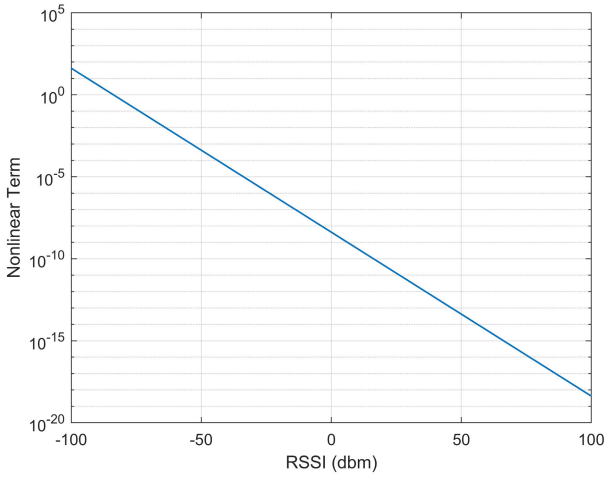


Fig. 6. Nonlinear term of the distance standard deviation formula.

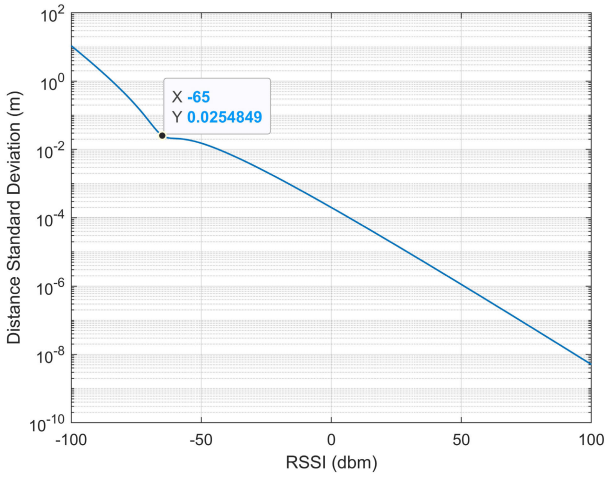


Fig. 7. Variation of distance standard deviation (σ_d) with respect to different RSSI values, including both linear and nonlinear terms.

2) Position Precision Estimation: After removing blunders and outliers from the raw RSSI measurements, the accuracy of the estimated receiver position with respect to the ground truth is presented in Table VI. Scenario 2 achieves higher accuracy

Authorized licensed use limited to: TU Delft Library. Downloaded on January 29,2026 at 11:10:50 UTC from IEEE Xplore. Restrictions apply.

TABLE VI
ROOT-MEAN-SQUARE ERROR (RMSE) OF THE ESTIMATED POSITION WITH RESPECT TO THE GROUND TRUTH

Position Accuracy	RMSE (m)
Scenario 1	0.1640
Scenario 2	0.0977

TABLE VII
ESTIMATED POSITIONING PRECISION FOR BOTH SCENARIOS

Position Precision	σ_{x_r}	σ_{y_r}	$\sigma_{x_r y_r}$
Scenario 1	0.7022	0.9398	-0.25
Scenario 2	0.6212	0.8158	-0.10

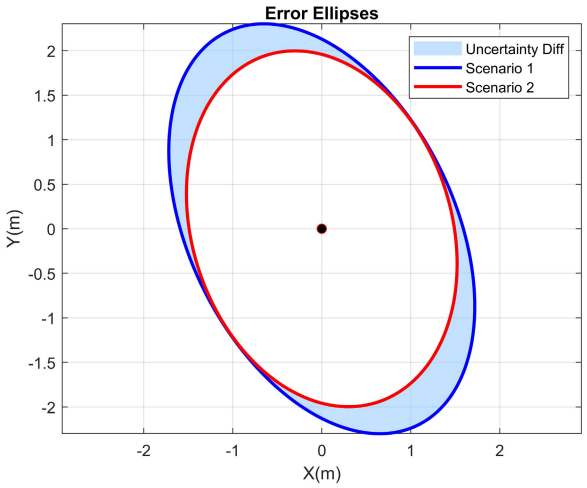


Fig. 8. Error ellipses of the receiver's estimated position in both scenarios, illustrating different uncertainty areas with a common center.

than Scenario 1, emphasizing the importance of sensor geometry. In Scenario 1, closely spaced beacons cause signal interference, complicating measurement separation. Multipath effects, high RSSI variability, blunders, and outliers further challenge the accurate obtainment of (3), often causing biased distance and position estimates. Therefore, experimental data should be smoothed and cleaned, as high precision can still coincide with low overall accuracy.

After calculating the distance precision, the position precision based on GDoP and distance precision is demonstrated in Table VII. To enhance the understanding of the uncertainty associated with an estimated position, the error ellipse serves as a particularly valuable analytical tool. It provides a visual representation of the uncertainty region, which is derived from the covariance matrix of the estimated unknown parameters [77], [78]. This graphical depiction allows for a more intuitive and comprehensive interpretation of positional uncertainty in relation to the statistical characteristics of the estimation process, as shown for our case in Figs. 8. As illustrated by the error ellipses corresponding to both scenarios, there is a clear distinction in the spatial extent of the uncertainties associated with the estimated receiver positions. Specifically, the error ellipse for Scenario 1 encompasses a significantly larger area compared to that of Scenario 2. This larger area reflects a broader spread in the positional estimates, which in turn implies lower precision in Scenario 1. Conversely, the smaller error ellipse observed in Scenario 2 suggests a more tightly clustered distribution of position estimates, indicating higher precision and more reliable localization performance.

The error ellipses have been constructed based on a 95% confidence level, meaning there is a 95% probability that the true receiver position lies within the bounds of each ellipse under the assumption of a bi-variate normal distribution of errors. Quantitatively, the area of the error ellipse in Scenario 1 is 23% greater than that in Scenario 2. This numerical difference further reinforces the observation that the uncertainty associated with the receiver's estimated position in Scenario 1 is substantially higher than in Scenario 2. Such a result highlights the superior accuracy and consistency of the positioning method or configuration employed in Scenario 2 relative to Scenario 1.

As discussed before, the computed results demonstrated that the precision of estimated positions in indoor environments using BLE beacons is significantly affected by two key factors. The first factor pertains to the uncertainty associated with the parameters of the mathematical model. Specifically, in scenarios where the receiver and transmitter are in close proximity, the estimated distances are more accurate, thereby enhancing the precision of the resulting positioning parameters. The second factor involves the geometry of sensor deployment. The spatial configuration between the receiver and transmitters has a direct influence on the uncertainty and overall accuracy of the positioning parameters. In particular, in centroid-based VT scenarios, this effect is clearly illustrated through the characteristics of the error ellipse. Moreover, the CVT represents a modified form of the classical VT that does not incur additional system costs. This is because the number of beacons remains the same, with only their positions being adjusted. Furthermore, the implementation cost exhibits no significant difference due to its structural similarity to the conventional VT.

V. CONCLUSION

In conclusion, this study identifies and analyzes two key components that govern the performance of BLE RSSI-based indoor positioning systems. The first component is the uncertainty in the mathematical model parameters, specifically the precision of the RSSI-distance model parameters—such as the environmental factor (ν) and the maximum power (μ) transmitted by the sensor at 1-m distance. These uncertainties can propagate to the positioning parameters' precision through the error propagation law. The second component is the geometry of sensor configuration in indoor spaces, which plays a crucial role in the precision of the estimated parameters. In this context, the GDoP serves as an important criterion for evaluating sensor deployment. Both components must be considered in the design and implementation of an indoor positioning system.

As a case study, two distinct BLE beacon sensor deployments were conducted in a metrology laboratory at Université Laval, Québec City, Canada, to demonstrate the impact of

Authorized licensed use limited to: TU Delft Library. Downloaded on January 29,2026 at 11:10:50 UTC from IEEE Xplore. Restrictions apply.

these on the final positioning outputs. One deployment followed the classical Voronoi Diagram approach (Scenario 1), while the other utilized a CVT approach (Scenario 2). The results show that Scenario 2, with a lower GDoP, provided higher precision compared to Scenario 1. However, the standard deviation of distances indicates that Scenario 1 offered better precision due to shorter distances between the beacons and the receiver.

The geometry of the sensor deployment affects the design matrix of unknown parameters (**A**) and the structure of the normal matrix (**N**). On the other hand, the uncertainty of the mathematical model influences the structure of the covariance matrix ($\mathbf{Q}_y$) and then the design matrix of observation (**B**). Ultimately, the precision of the positioning parameters is determined by the combination of these components. In the case studies, the impact of GDoP (on the normal matrix) and distance-related uncertainty is specifically addressed.

Finally, this study focuses on the precision of distance and position estimates rather than their accuracy. While accuracy remains an important consideration in indoor positioning applications, the present work emphasizes the precision of the resulting measurements.

ACKNOWLEDGMENT

The authors would like to express their gratitude to the Canada Research Chair in Senseable Cities for Empowered Mobilities through the Natural Sciences and Engineering Research Council of Canada (NSERC) for providing the BLE beacon and surveying equipment used to conduct the precise measurements. They also wish to sincerely thank Dr. Christian Larouche from the Department of Geomatic Sciences at Université Laval for his invaluable assistance in facilitating the necessary conditions for this work.

REFERENCES

[1] T.-M.-T. Dinh, N.-S. Duong, and K. Sandrasegaran, "Smartphone-based indoor positioning using BLE iBeacon and reliable lightweight fingerprint map," *IEEE Sensors J.*, vol. 20, no. 17, pp. 10283–10294, Sep. 2020.

[2] T.-M.-T. Dinh, N.-S. Duong, and Q.-T. Nguyen, "Developing a novel real-time indoor positioning system based on BLE beacons and smartphone sensors," *IEEE Sensors J.*, vol. 21, no. 20, pp. 23055–23068, Oct. 2021.

[3] W. Xue, W. Qiu, X. Hua, and K. Yu, "Improved Wi-Fi RSSI measurement for indoor localization," *IEEE Sensors J.*, vol. 17, no. 7, pp. 2224–2230, Apr. 2017.

[4] X. Chen and S. Zou, "Improved Wi-Fi indoor positioning based on particle swarm optimization," *IEEE Sensors J.*, vol. 17, no. 21, pp. 7143–7148, Nov. 2017.

[5] C.-Y. Yao and W.-C. Hsia, "An indoor positioning system based on the dual-channel passive RFID technology," *IEEE Sensors J.*, vol. 18, no. 11, pp. 4654–4663, Jun. 2018.

[6] M. Merenda, L. Catarinucci, R. Colella, D. Iero, F. G. D. Corte, and R. Carotenuto, "RFID-based indoor positioning using edge machine learning," *IEEE J. Radio Freq. Identificat.*, vol. 6, pp. 573–582, 2022.

[7] P. Dabove, V. Di Pietra, M. Piras, A. A. Jabbar, and S. A. Kazim, "Indoor positioning using ultra-wide band (UWB) technologies: Positioning accuracies and sensors' performances," in *Proc. IEEE/ION Position, Location Navigat. Symp. (PLANS)*, Apr. 2018, pp. 175–184.

[8] X. Yang, J. Wang, D. Song, B. Feng, and H. Ye, "A novel NLOS error compensation method based IMU for UWB indoor positioning system," *IEEE Sensors J.*, vol. 21, no. 9, pp. 11203–11212, May 2021.

[9] A. Bensky, *Wireless Positioning Technologies and Applications*. Norwood, MA, USA: Artech House, 2016.

[10] Y. Zhuang, C. Zhang, J. Huai, Y. Li, L. Chen, and R. Chen, "Bluetooth localization technology: Principles, applications, and future trends," *IEEE Internet Things J.*, vol. 9, no. 23, pp. 23506–23524, Dec. 2022.

[11] C. Yang and H.-R. Shao, "WiFi-based indoor positioning," *IEEE Commun. Mag.*, vol. 53, no. 3, pp. 150–157, Mar. 2015.

[12] G. Retscher and Q. Fu, "Continuous indoor navigation with RFID and INS," in *Proc. IEEE/ION Position, Location Navigat. Symp.*, May 2010, pp. 102–112.

[13] S. S. Saab and Z. S. Nakad, "A standalone RFID indoor positioning system using passive tags," *IEEE Trans. Ind. Electron.*, vol. 58, no. 5, pp. 1961–1970, May 2011.

[14] F. Mazhar, M. G. Khan, and B. Sällberg, "Precise indoor positioning using UWB: A review of methods, algorithms and implementations," *Wireless Pers. Commun.*, vol. 97, no. 3, pp. 4467–4491, Dec. 2017.

[15] J. Yan, D. Lin, K. Tang, G. Yang, and Q. Ye, "High precision indoor positioning method based on UWB," in *Proc. 11th EAI Int. Conf. Ad Hoc Netw.*, Queenstown, New Zealand, Nov. 2019, pp. 201–207.

[16] Z. Jianyong, L. Haiyong, C. Zili, and L. Zhaohui, "RSSI based Bluetooth low energy indoor positioning," in *Proc. Int. Conf. Indoor Positioning Indoor Navigat. (IPIN)*, Oct. 2014, pp. 526–533.

[17] Y. Assayag, H. Oliveira, E. Souto, R. Barreto, and R. Pazzi, "Adaptive path loss model for BLE indoor positioning system," *IEEE Internet Things J.*, vol. 10, no. 14, pp. 12898–12907, Jul. 2023.

[18] Y. Zhuang, J. Yang, Y. Li, L. Qi, and N. El-Sheimy, "Smartphone-based indoor localization with Bluetooth low energy beacons," *Sensors*, vol. 16, no. 5, p. 596, Apr. 2016.

[19] V. C. Paterna, A. C. Augé, J. P. Aspas, and M. P. Bullones, "A Bluetooth low energy indoor positioning system with channel diversity, weighted trilateration and Kalman filtering," *Sensors*, vol. 17, no. 12, p. 2927, Dec. 2017.

[20] J. Röbesaat, P. Zhang, M. Abdelaal, and O. Theel, "An improved BLE indoor localization with Kalman-based fusion: An experimental study," *Sensors*, vol. 17, no. 5, p. 951, Apr. 2017.

[21] Y. Assayag, H. Oliveira, E. Souto, R. Barreto, and R. Pazzi, "A model-based BLE indoor positioning system using particle swarm optimization," *IEEE Sensors J.*, vol. 24, no. 5, pp. 6898–6908, Mar. 2024.

[22] X. Hou and T. Arslan, "Monte Carlo localization algorithm for indoor positioning using Bluetooth low energy devices," in *Proc. Int. Conf. Localization GNSS (ICL-GNSS)*, Jun. 2017, pp. 1–6.

[23] X. Hou, T. Arslan, and J. Gu, "Indoor localization for Bluetooth low energy using wavelet and smoothing filter," in *Proc. Int. Conf. Localization GNSS (ICL-GNSS)*, Jun. 2017, pp. 1–6.

[24] P. Sthapit, H.-S. Gang, and J.-Y. Pyun, "Bluetooth based indoor positioning using machine learning algorithms," in *Proc. IEEE Int. Conf. Consum. Electron. - Asia (ICCE-Asia)*, Jun. 2018, pp. 206–212.

[25] A. Nessa, B. Adhikari, F. Hussain, and X. N. Fernando, "A survey of machine learning for indoor positioning," *IEEE Access*, vol. 8, pp. 214945–214965, 2020.

[26] F. Ye, R. Chen, G. Guo, X. Peng, Z. Liu, and L. Huang, "A low-cost single-anchor solution for indoor positioning using BLE and inertial sensor data," *IEEE Access*, vol. 7, pp. 162439–162453, 2019.

[27] Y. Yu et al., "A novel 3-D indoor localization algorithm based on BLE and multiple sensors," *IEEE Internet Things J.*, vol. 8, no. 11, pp. 9359–9372, Jun. 2021.

[28] C. S. Mouhammad, A. Allam, M. Abdel-Raouf, E. Shenouda, and M. Elsabrouty, "BLE indoor localization based on improved RSSI and trilateration," in *Proc. 7th Int. Jpn.-Afr. Conf. Electron., Commun., Computations, (JAC-ECC)*, Dec. 2019, pp. 17–21.

[29] R. W. C. Ling, A. Gupta, A. Vashistha, M. Sharma, and C. L. Law, "High precision UWB-IR indoor positioning system for IoT applications," in *Proc. IEEE 4th World Forum Internet Things (WF-IoT)*, Feb. 2018, pp. 135–139.

[30] H. Guo, M. Li, X. Zhang, Q. Liu, and X. Gao, "Research on indoor wireless positioning precision optimization based on UWB," *J. Web Eng.*, vol. 19, nos. 7–8, pp. 1017–1048, Dec. 2020.

[31] H. Zhang, Q. Wang, Z. Li, J. Mi, and K. Zhang, "Research on high precision positioning method for pedestrians in indoor complex environments based on UWB/IMU," *Remote Sens.*, vol. 15, no. 14, p. 3555, Jul. 2023.

Authorized licensed use limited to: TU Delft Library. Downloaded on January 29,2026 at 11:10:50 UTC from IEEE Xplore. Restrictions apply.

[32] Z. Yin, X. Jiang, Z. Yang, N. Zhao, and Y. Chen, "WUB-IP: A high-precision UWB positioning scheme for indoor multiuser applications," *IEEE Syst. J.*, vol. 13, no. 1, pp. 279–288, Mar. 2019.

[33] N. Bai, Y. Tian, Y. Liu, Z. Yuan, Z. Xiao, and J. Zhou, "A high-precision and low-cost IMU-based indoor pedestrian positioning technique," *IEEE Sensors J.*, vol. 20, no. 12, pp. 6716–6726, Jun. 2020.

[34] S. Yang, L. Ma, S. Jia, and D. Qin, "An improved vision-based indoor positioning method," *IEEE Access*, vol. 8, pp. 26941–26949, 2020.

[35] Á. De-La-Llana-Calvo, D. Salido-Monzú, J.-L. Lázaro-Galilea, A. Gardel-Vicente, I. Bravo-Muñoz, and B. Rubiano-Muriel, "Accuracy and precision assessment of AoA-based indoor positioning systems using infrastructure lighting and a position-sensitive detector," *Sensors*, vol. 20, no. 18, p. 5359, Sep. 2020.

[36] Y. Cai, W. Guan, Y. Wu, C. Xie, Y. Chen, and L. Fang, "Indoor high precision three-dimensional positioning system based on visible light communication using particle swarm optimization," *IEEE Photon. J.*, vol. 9, no. 6, pp. 1–20, Dec. 2017.

[37] X. Gan et al., "A new array pseudolites technology for high precision indoor positioning," *IEEE Access*, vol. 7, pp. 153269–153277, 2019.

[38] Y. Zhao et al., "A new method of high-precision positioning for an indoor pseudolite without using the known point initialization," *Sensors*, vol. 18, no. 6, p. 1977, Jun. 2018.

[39] P. Grasso, M. S. Innocente, J. J. Tai, O. Haas, and A. M. Dizqah, "Analysis and accuracy improvement of UWB-TDoA-based indoor positioning system," *Sensors*, vol. 22, no. 23, p. 9136, Nov. 2022.

[40] J.-H. Seong, S.-H. Lee, W.-Y. Kim, and D.-H. Seo, "High-precision RTT-based indoor positioning system using RCDN and RPN," *Sensors*, vol. 21, no. 11, p. 3701, May 2021.

[41] K. Gao, H. Wang, H. Lv, and W. Liu, "Toward 5G NR high-precision indoor positioning via channel frequency response: A new paradigm and dataset generation method," *IEEE J. Sel. Areas Commun.*, vol. 40, no. 7, pp. 2233–2247, Jul. 2022.

[42] J. Qiao, F. Yang, J. Liu, G. Huang, W. Zhang, and M. Li, "Advancements in indoor precision positioning: A comprehensive survey of UWB and Wi-Fi RTT positioning technologies," *Network*, vol. 4, no. 4, pp. 545–566, Nov. 2024.

[43] M. Elsanhoury et al., "Precision positioning for smart logistics using ultra-wideband technology-based indoor navigation: A review," *IEEE Access*, vol. 10, pp. 44413–44445, 2022.

[44] J. Barnes, C. Rizos, J. Wang, D. Small, G. Voigt, and N. Gambale, "Locata: A new positioning technology for high precision indoor and outdoor positioning," in *Proc. 16th Int. Tech. Meeting Satell. Division Inst. Navigat. (ION GPS/GNSS)*, Jul. 2003, pp. 1119–1128.

[45] A. Ozer and E. John, "Improving the accuracy of Bluetooth low energy indoor positioning system using Kalman filtering," in *Proc. Int. Conf. Comput. Sci. Comput. Intell. (CSCI)*, Dec. 2016, pp. 180–185.

[46] R. B. Langley et al., "Dilution of precision," *GPS World*, vol. 10, no. 5, pp. 52–59, 1999.

[47] A. Dwi Ramadhani, P. Kristalina, and A. Sudarsono, "A weighted geometric dilution of precision-based method for indoor positioning system," *J. Commun.*, pp. 65–73, Jan. 2020.

[48] M. Wang, Z. Chen, Z. Zhou, J. Fu, and H. Qiu, "Analysis of the applicability of dilution of precision in the base station configuration optimization of ultrawideband indoor TDOA positioning system," *IEEE Access*, vol. 8, pp. 225076–225087, 2020.

[49] I. Sharp, K. Yu, and M. Hedley, "On the GDOP and accuracy for indoor positioning," *IEEE Trans. Aerosp. Electron. Syst.*, vol. 48, no. 3, pp. 2032–2051, Jul. 2012.

[50] K. Küçük, "Horizontal dilution of precision-based ultra-wideband positioning technique for indoor environments," *Turkish J. Electr. Eng. Comput. Sci.*, vol. 22, pp. 1307–1322, Aug. 2014.

[51] A. Albaidhani and A. Alsudani, "Anchor selection by geometric dilution of precision for an indoor positioning system using ultra-wide band technology," *IET Wireless Sensor Syst.*, vol. 11, no. 1, pp. 22–31, Feb. 2021.

[52] J. J. Khalife and Z. Z. M. Kassas, "Optimal sensor placement for dilution of precision minimization via quadratically constrained fractional programming," *IEEE Trans. Aerosp. Electron. Syst.*, vol. 55, no. 4, pp. 2086–2096, Aug. 2019.

[53] Y. Guo, W. Li, G. Yang, Z. Jiao, and J. Yan, "Combining dilution of precision and Kalman filtering for UWB positioning in a narrow space," *Remote Sens.*, vol. 14, no. 21, p. 5409, Oct. 2022.

[54] Q. Wang, B. Li, and C. Rizos, "Dilution of precision in three dimensional angle-of-arrival positioning systems," *J. Electr. Eng. Technol.*, vol. 14, no. 6, pp. 2583–2593, Nov. 2019.

[55] J. Zhang and J. Lu, "Analytical evaluation of geometric dilution of precision for three-dimensional angle-of-arrival target localization in wireless sensor networks," *Int. J. Distrib. Sensor Netw.*, vol. 16, no. 5, May 2020, Art. no. 155014772092047.

[56] Z. Hao, J. Dang, Y. Yan, and X. Wang, "A node localization algorithm based on Voronoi diagram and support vector machine for wireless sensor networks," *Int. J. Distrib. Sensor Netw.*, vol. 17, no. 2, Feb. 2021, Art. no. 155014772199341.

[57] J. D. Hobby and M. Dashti, "A method to incorporate floor plan constraints into indoor location tracking: A Voronoi approach," *Mobile Inf. Syst.*, vol. 2018, pp. 1–11, 2018.

[58] Y. F. Yong, C. K. Tan, I. K. T. Tan, and S. W. Tan, "Radio map construction using fingerprints clustering and Voronoi diagram for indoor positioning," in *Proc. 21st Int. Symp. Commun. Inf. Technol. (ISCIT)*, Sep. 2022, pp. 64–69.

[59] X. Yang, F. Yan, and J. Liu, "3D localization algorithm based on Voronoi diagram and rank sequence in wireless sensor network," *Sci. Program.*, vol. 2017, pp. 1–8, Sep. 2017.

[60] A. Afghantoloee and M. A. Mostafavi, "A local 3D Voronoi-based optimization method for sensor network deployment in complex indoor environments," *Sensors*, vol. 21, no. 23, p. 8011, Nov. 2021.

[61] S. Friedman, H. Pasula, and D. Fox, "Voronoi random fields: Extracting topological structure of indoor environments via place labeling," in *Proc. IJCAI*, vol. 7, 2007, pp. 2109–2114.

[62] K. Onishi, "Indoor position detection using BLE signals based on Voronoi diagram," in *Proc. Int. Conf. Intell. Softw. Methodologies*, 2015, pp. 18–29.

[63] Q. Du, V. Faber, and M. Gunzburger, "Centroidal Voronoi tessellations: Applications and algorithms," *SIAM Rev.*, vol. 41, no. 4, pp. 637–676, Jan. 1999.

[64] Q. Du and M. Gunzburger, "Grid generation and optimization based on centroidal Voronoi tessellations," *Appl. Math. Comput.*, vol. 133, nos. 2–3, pp. 591–607, Dec. 2002.

[65] L. Ju, Q. Du, and M. Gunzburger, "Probabilistic methods for centroidal Voronoi tessellations and their parallel implementations," *Parallel Comput.*, vol. 28, no. 10, pp. 1477–1500, Oct. 2002.

[66] Q. Du and D. Wang, "The optimal centroidal Voronoi tessellations and the gersho's conjecture in the three-dimensional space," *Comput. Math. Appl.*, vol. 49, nos. 9–10, pp. 1355–1373, May 2005.

[67] Q. Du, M. D. Gunzburger, and L. Ju, "Constrained centroidal Voronoi tessellations for surfaces," *SIAM J. Sci. Comput.*, vol. 24, no. 5, pp. 1488–1506, Jan. 2003.

[68] Q. Du, M. Emelianenko, and L. Ju, "Convergence of the Lloyd algorithm for computing centroidal Voronoi tessellations," *SIAM J. Numer. Anal.*, vol. 44, no. 1, pp. 102–119, Jan. 2006.

[69] Y. Liu et al., "On centroidal Voronoi tessellation—Energy smoothness and fast computation," *ACM Trans. Graph.*, vol. 28, no. 4, pp. 1–17, Aug. 2009.

[70] B. Lévy and Y. Liu, "L p centroidal Voronoi tessellation and its applications," *ACM Trans. Graph.*, vol. 29, no. 4, pp. 1–11, Jul. 2010.

[71] K. O. Arras, "An introduction to error propagation: Derivation, meaning and examples of equation CY= FX CX FXT," Auton. Syst. Lab, Inst. Robotic Syst., Swiss Federal Inst. Technol. Lausanne (EPFL), Tech. Rep. EPFL-ASL-TR-98-01 R3, Sep. 1998.

[72] G. Li, E. Geng, Z. Ye, Y. Xu, J. Lin, and Y. Pang, "Indoor positioning algorithm based on the improved RSSI distance model," *Sensors*, vol. 18, no. 9, p. 2820, Aug. 2018.

[73] M. M. Kariminejad, M. A. Sharifi, and A. R. Amiri-Simkooei, "Tikhonov-regularized weighted total least squares formulation with applications to geodetic problems," *Acta Geodaetica et Geophysica*, vol. 57, no. 1, pp. 23–42, Mar. 2022.

[74] B. Schaffrin and K. Snow, "Total least-squares regularization of tykhonov type and an ancient racetrack in corinth," *Linear Algebra Appl.*, vol. 432, no. 8, pp. 2061–2076, Apr. 2010.

[75] P. J. Teunissen, *Adjustment Theory: An Introduction*. Delft, The Netherlands: TU Delft Open Publishing, 2024.

[76] Q. Du, M. Gunzburger, and L. Ju, "Advances in studies and applications of centroidal Voronoi tessellations," *Numer. Math., Theory, Methods Appl.*, vol. 3, no. 2, pp. 119–142, 2010.

[77] W. E. Hoover, "Algorithms for confidence circles and ellipses," U.S. Dept. Commerce, Nat. Ocean. Atmos. Admin., National Ocean Service, NOAA Tech. Rep. NOS 107 C&GS 3, Sep. 1984.

[78] S. Zaminpardaz and P. J. G. Teunissen, "On the computation of confidence regions and error ellipses: A critical appraisal," *J. Geodesy*, vol. 96, no. 2, p. 10, Feb. 2022.

Authorized licensed use limited to: TU Delft Library. Downloaded on January 29,2026 at 11:10:50 UTC from IEEE Xplore. Restrictions apply.



Mohammad Mahdi Kariminejad (Member, IEEE) received the B.Sc. degree in civil surveying engineering and the M.Sc. degree in geodesy engineering from the University of Tehran, Tehran, Iran, in 2017 and 2020, respectively, where he is currently pursuing the Ph.D. degree in geodesy engineering with the Department of Geospatial and Surveying Engineering.

He is a Visiting Ph.D. Student at the Department of Geomatic Sciences, Université Laval, Québec City, QC, Canada. He is affiliated with Canada Research Chair in Senseable Cities for Empowered Mobilities and the Center for Research in Geospatial Data and Intelligence (CRDIG), Québec City. His research interests include wireless positioning, indoor navigation, GNSS–INS integration, sensor calibration, and multisensor fusion for navigation in smart cities, urban canyons, and indoor environments.



Mohammad Ali Sharifi (Member, IEEE) received the Ph.D. degree in satellite geodesy from the University of Stuttgart, Stuttgart, Germany, in 2006.

He is a Full Professor at the Department of Geospatial and Surveying Engineering, Faculty of Engineering, University of Tehran, Tehran, Iran. He is also an expert in satellite orbit determination, with particular emphasis on the kinematic orbit determination of low Earth orbit (LEO) satellites. In addition, he has conducted extensive research on the application of numerical optimization techniques to a wide range of terrestrial and space geodetic problems. His research focuses on improving the accuracy and precision of positioning and navigation for low-cost devices through advanced mathematical methods.



Alireza Amiri-Simkooei (Member, IEEE) received the Ph.D. degree in mathematical geodesy from Delft University of Technology (TU Delft), Delft, South Holland, The Netherlands, in 2007.

He is an Associate Professor with the Department of Control and Operations, Faculty of Aerospace Engineering, TU Delft. He has authored or co-authored more than 100 peer-reviewed research articles in ISI-indexed journals. His research interests include aviation acoustics, machine learning, advanced estimation and approximation methods, precise positioning using space-based systems, and the analysis of noise characteristics in geoscience data series. His work also focuses on least-squares variance component estimation and its applications to GPS time series.



Mir Abolfazl Mostafavi (Member, IEEE) is a Full Professor with the Department of Geomatic Sciences, Université Laval, Québec City, QC, Canada. He holds a Canada Research Chair in Senseable Cities for Empowered Mobilities. His research interests include the development of advanced geospatial information theories, methods, and tools that integrate geographic information science (GIS), GPS, wireless sensor networks (WSNs), the Internet of Things (IoT), digital twins, and artificial intelligence (AI) to address challenges related to sustainable and inclusive mobility in the context of smart cities.

Dr. Mostafavi is a member of the Center for Research in Geospatial Data and Intelligence (CRDIG) and the Center for Interdisciplinary Research in Rehabilitation and Social Integration (CIRRIS).

Authorized licensed use limited to: TU Delft Library. Downloaded on January 29,2026 at 11:10:50 UTC from IEEE Xplore. Restrictions apply.